The Visual Computer (2020) 36:2201–2214
https://doi.org/10.1007/s00371-020-01909-2

ORIGINAL ARTICLE

Robust and blind image watermarking via circular embedding and bidimensional empirical mode decomposition

Xiaochao Wang[1] · Kun Hu[2] · Jianping Hu[3] · Ling Du[1] · Anthony T. S. Ho[4] · Hong Qin[5]

Published online: 16 July 2020

Abstract
In this paper, a robust and blind image watermarking algorithm via circular embedding and bidimensional empirical mode decomposition (BEMD) is developed. First, the watermark image is scrambled by Arnold transform to increase the security of the algorithm. Second, the Hilbert curve is adopted to reduce the scrambled 2D watermark image to one-dimensional watermark signal. Third, the host image is decomposed by BEMD to obtain the multi-scale representation in the forms of intrinsic mode functions (IMFs) and a residue. Then, the extreme points of the IMFs are extracted as the embedding locations. Finally, the one-dimensional watermark signal is repeatedly and cyclically embedded in the extreme locations of the first IMF according to the texture masking characteristics of the human visual system, which greatly improves the ability of our algorithm against various attacks. The final watermarked image is reconstructed by combining the modified first IMF and the residual. The watermark can be successfully extracted without resorting to the original host image. Furthermore, image correction can be applied before image watermarking extraction if there are geometric attacks in watermarked image. A large number of experimental results and thorough evaluations confirm that our method can obtain higher imperceptibility and robustness under different types of attacks, and achieve better performance than the current state-of-the-art watermarking algorithms, especially in large-scale cropping attack, JPEG compression, Gaussian noise, sharpening, Gamma correction, scaling, histogram equalization, and rotation attacks.

Keywords Image watermarking · Circular embedding · BEMD · Arnold transform · Hilbert curve

1 Introduction and motivation

With the widespread popularity of image acquisition equipments and the rapid development of digital media communication technologies, magnanimous images could be easily acquired, duplicated, revised, and disseminated. Apart from these conveniences, the abuse of images, copyright infringement, malicious dissemination have arisen and attracted extensive attentions in the area of digital media and information technologies. To solve the aforementioned issue and protect the copyright of images, image watermarking has been widely studied as a very promising information security technology and plays an important role in protecting the copyright of digital images.

✉ Jianping Hu
neduhjp307@163.com

Xiaochao Wang
wangxiaochao18@163.com

Kun Hu
ucas_hukun@163.com

Ling Du
duling@tiangong.edu.cn

Anthony T. S. Ho
a.ho@surrey.ac.uk

Hong Qin
qin@cs.stonybrook.edu

[1] School of Mathematical Sciences, Tiangong University, Tianjin 300387, China

[2] University of Chinese Academy of Sciences, Beijing 100049, China

[3] School of Sciences, Northeast Electric Power University, Jilin 132012, China

[4] Department of Computer Science, University of Surrey, Guildford, Surrey GU2 7XH, UK

[5] Department of Computer Science, Stony Brook University, Stony Brook, NY 11794-4400, USA

Recently, a powerful tool for processing non-stationary and nonlinear one-dimensional signals, named empirical mode decomposition (EMD), has been proposed and widely studied in signal processing. EMD has also been extended to two-dimensional image processing and adopted in image watermarking algorithms [1,2,7,27]. Although EMD has been extended and adopted in watermarking algorithms, there are still many limitations yet to be addressed. First, embedding watermarks in sub-images may result in visual block effects, and the size matching between the watermark image and the sub-images limits the application scope of the algorithms [1,7,27]. Second, the original host images are utilized in watermark extraction process [1,2,27], which might not be available in most cases. Third, randomly modifying the IMFs [2] gives rise to lower imperceptibility and less robustness against attacks. More seriously, all of these algorithms are feeble against geometric attacks, such as rotating, cropping, and scaling.

To overcome the aforementioned limitations, a robust and blind image watermarking algorithm via circular embedding and BEMD is developed in this paper. Watermark image is first scrambled by Arnold transform to increase its security. Then, the Hilbert curve is adopted to reduce the two-dimensional scrambled watermark image into a one-dimensional watermark signal. For the host image, instead of dividing it into sub-images, it is directly decomposed by BEMD to obtain the multi-scale representation, which can avoid the visual block effects across the boundaries of sub-images.

According to texture masking characteristics of HVS, it is natural to embed the watermark into the regions with rich textures. For that, the prepared one-dimensional watermark signal is repeatedly and circularly embedded into the extremum positions of the first IMF, which greatly improves the ability of our algorithm against various attacks. The final watermarked image is obtained by combining the modified first IMF and the residual. In the watermark extraction stage, the watermark can be successfully extracted without the original host image. Moreover, image correction can be optionally applied before watermark extraction if watermarked images are attacked by geometric attacks. The pipeline of our watermarking framework is illustrated in Fig. 1.

The salient contributions of this paper can be summarized as follows:

- Hilbert curve is utilized to transform the watermark image of any size and any dimension to one dimension signal, which scrambles the watermark and enhances the security of the algorithm. Moreover, this dimension reduction strategy not only solves the problem of size matching between watermark image and host image, but also avoids the block artifacts suffered in most watermarking algorithms.
- Watermarks are embedded into the extremum positions of the first IMF by considering the HVS characteristics of texture masking. This embedding scheme enables our method to produce higher imperceptibility, robustness, and less distortion than previous BEMD-based watermarking algorithms, in which the watermarks are simply embedded into the residue or randomly embedded in different IMFs.
- Robust and blind image watermarking algorithm is developed via the circular embedding and BEMD. The circular embedding strategy increases the embedding capacity and enhances the robustness of the algorithm against various attacks, especially for large-scale shear attack, JPEG compression. Optional image correction further enables the algorithm to combat geometric attacks.

2 Related works

In this section, traditional watermarking algorithms, hybrid watermarking algorithms, and BEMD-based watermarking algorithms are briefly reviewed.

Traditional Watermarking Algorithms. Traditional watermarking algorithms can be generally divided into two categories, spatial domain-based methods and the transform domain methods. The spatial domain-based methods directly embed the watermark into the host image and modify its pixel values slightly. One well-known spatial domain-based method is embedding the watermark in the least significant bit of host image pixels [8,12]. Generally speaking, spatial domain-based methods have low computational complexity, however, they are not robust against most attacks.

In contrast, the transform domain-based methods transform the host image into frequency domain and the watermark is embedded by modifying the frequency coefficients of host image. The widely studied transform domain-based methods include discrete Fourier transform (DFT) [9,30,32], discrete cosine transform (DCT) [5,10,28], discrete wavelet transform (DWT) [3,23,37], and singular value decomposition (SVD) [14,21,22]. In contrast to spatial domain-based methods, the transform-based methods are relatively more robust to the image processing and most attacks, even though they usually require complex computation.

Hybrid Watermarking Algorithms. Combining the existing technologies, hybrid watermarking algorithms [15,24,26] have been rapidly developed in recent years. To balance the tradeoff between imperceptibility and robustness of the watermarking algorithm, Roy and Pal [24] proposed a blind image watermarking algorithm based on Redundant DWT

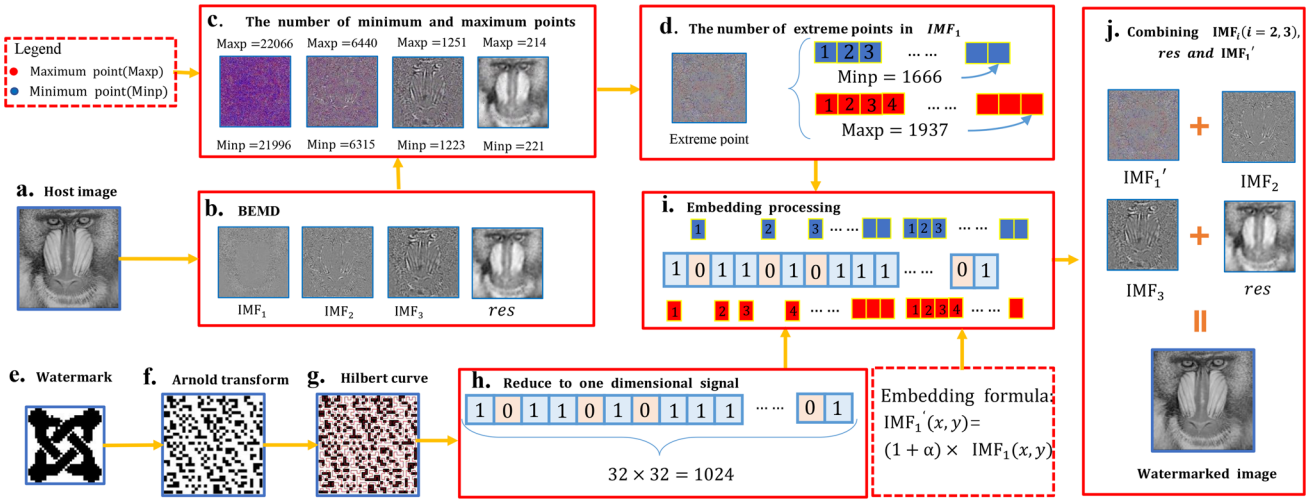

Fig. 1 The pipeline of watermark embedding. **a** Host image. **b** BEMD with the obtained three IMFs and a residue. **c** The number of minimum and maximum points of each layer. **d** Number of extreme points in IMF_1. **e** Watermark image. **f** Arnold transform. **g** Hilbert curve. **h** One-dimensional signal. **i** Embedding processing. **j** Final watermarked image

and DCT, while Mohamed et al. [15] put forward a blind hybrid image watermarking method by using DFT and DCT.

Taking advantage of amplified pseudo-noise strings, discrete curvelet transform, and DCT transform, a blind watermarking algorithm is proposed in [26]. These hybrid watermarking algorithms are resistant to the common image watermarking attacks; nonetheless, they are still not robust to geometric attacks, especially rotation attack. In addition, the computational complexity of these hybrid watermarking algorithms is extremely higher because we have to combine several transform domain techniques together.

BEMD-Based Watermarking Algorithms. Apart from the traditional and hybrid watermarking algorithms, BEMD-based watermarking algorithms [1,2,7,27] have drawn more and more attention. Sabri et al. [2] proposed a non-blind watermarking method by using a secret key to randomly select a sequence of pixels in each IMF to be modified. Randomly modifying the IMFs of host image reduces the imperceptibility of the algorithm. In [27], host image is first decomposed into several self-fractional Fourier function images, then these images are further decomposed into IMFs using BEMD. Finally, watermarks are embedded in the residue of decomposed image. Abbas et al. [1] proposed an image watermarking method based on lifting wavelet transform, DWT, and BEMD. Combining three decomposition methods causes the (new) algorithms of high computation complexity. These algorithms are non-blind algorithms, and original image should be provided in watermark extraction.

Bi et al. [7] proposed a blind image watermarking algorithm based on wavelet transformation and EMD. Host image is first divided into non-overlapped sub-blocks, then the watermark is embedded in the mean trend of middle frequency sub-images in the wavelet domain. These algorithms have worse performance under geometric attacks such as rotating, translating, and scaling. Moreover, dividing the original image into sub-images requires the size of the watermark image should match with the size of the sub-images, which limits the application scope of these methods.

3 New algorithm

3.1 Overview of watermark embedding

Given a gray image $\mathbf{I}(x, y)$ with the size $m \times n$ as the host image and a binary watermark image $\mathbf{W}(x, y)$ with the size $N \times N$, Fig. 1 illustrates the pipeline of our new algorithm by taking the Baboon as a host image and the Unity as the watermark image. For the watermark image $\mathbf{W}(x, y)$ (Fig. 1e), it is first scrambled by Arnold transform to increase the security of the algorithm, and the scrambled image $\mathbf{W}_a(x, y)$ is obtained (Fig. 1f), which will be further transformed into one-dimensional signal $\mathbf{W}_h$ (Fig. 1h) using Hilbert curve (Fig. 1g). For the host image $\mathbf{I}(x, y)$ (Fig. 1a), it is decomposed into multi-scale representation of IMFs and a residue by BEMD (Fig. 1b). After that the extreme points are extracted from the IMFs (Fig. 1c) and the embedding positions are eventually selected in the first IMF. Then, $\mathbf{W}_h$ is circularly embedded in the first IMF at the extreme positions (Fig. 1i). Finally, the watermarked image $\mathbf{I}_w(x, y)$ (Fig. 1j) is obtained by combining the modified first IMF with other IMFs and the residue.

3.2 Preprocessing

Encryption via the Arnold Transform. To enhance the robustness and security of watermark image, the watermark image is first permuted by Arnold transform before embedding. For watermark image $\mathbf{W}(x, y)$ and the pixels' positions $\{(x, y)|x, y = 0, 1, 2, \ldots, N-1\}$, Arnold transform is formulated as

$$\begin{pmatrix} x' \\ y' \end{pmatrix} = \begin{pmatrix} 1 & 1 \\ 1 & 2 \end{pmatrix} \begin{pmatrix} x \\ y \end{pmatrix} \bmod(N), \tag{1}$$

where x' and y', respectively, represents the position after shifting from the original position of x and y, N is the size of watermark image, $mod(N)$ denotes the modulus operation (divided by N). This is an iterative process by moving pixels' positions several times and returning to original position after T iterations, which is the period of Arnold scrambling. After Arnold transform, the correlations between the image pixels are damaged and no meaningful information can be directly observed. Figure 1e–f shows a watermark image and the result after Arnold transform.

Conventionally, the encrypted image could be recovered to the original image by performing $T - H$ iterations, if H scrambling iterations have been applied on the watermark image. In principle, the image can be effectively restored by the inverse Arnold transformation, which is defined as

$$\begin{pmatrix} x \\ y \end{pmatrix} = \begin{pmatrix} 2 & -1 \\ -1 & 1 \end{pmatrix} \begin{pmatrix} x' \\ y' \end{pmatrix} \bmod(N). \tag{2}$$

Dimensional Reduction. Hilbert curve was first developed by David Hilbert [17] and is one type of space-filling curve in two-dimensional space which passes through all the points once and only once in certain predefined order. Comparing with other kinds of space-filling curves, such as Z-curve, Peano curve, and Gosper curve, Hilbert curve enjoys strong local properties, making it more suitable in image processing. Hilbert curve is a continuous curve and can be viewed as a continuous, surjective and nowhere differentiable function [25], which maps a higher-dimensional space into a one-dimensional space

$$f : \{1, \ldots, n\}^d \mapsto \{1, \ldots, n^d\}. \tag{3}$$

The mapping from multidimensional space to one-dimensional space of Hilbert curve induces a natural dimension reduction from a 2D image to one-dimensional signal. Motivated by this observation, Hilbert curve is adopted to solve the problem of size matching between the watermark image with the host image. Before the watermark embedding, the encrypted watermark image is first transformed to one-dimensional signal. Since the pixels of scrambled watermark image are placed in a sequence according to the order of Hilbert curve passing through them, therefore, the security of the watermark image is further enhanced. Figure 1g, h shows the Hilbert curve and the reduced one-dimensional signal.

Bidimensional Empirical Mode Decomposition. EMD was first proposed in [20] and had become an effective and powerful tool for analysing nonlinear and non-stationary signals. It decomposes the signal into a finite sum of frequency components, named IMFs and a residue, which are ranging from higher frequency to lower frequency. Unlike traditional Fourier and wavelet transform methods, which usually decompose a signal into different scales using predefined basis functions, while EMD expresses a signal as expansion of IMFs, which is a fully adaptive and data-driven decomposition algorithm. For its good properties and ease of implementation, EMD has captured much attention and has been widely applied in 1D signal processing [13,20], 2D image processing [29,38] and 3D geometry processing [18,19,33–36,39].

BEMD is a natural generalization of one-dimensional EMD for two-dimensional image processing. Similar to one-dimensional EMD, BEMD is also achieved by the sifting processing, which involves the main steps of local extreme point extraction, envelope computation, and stopping criteria of the sifting. Since cubic spline is a tool for constructing upper and lower envelopes of signals in one-dimensional EMD, its natural extension in two-dimensional Euclidean space is thin-plate spline. It is obtained by minimizing the energy of thin plates subject to certain data constraints and has witnessed important applications in data interpolation and approximation. Different from previous thin-plate spline interpolation methods, following the idea of [18,33], the energy minimization problem of thin-plate spline is transformed by solving the sparse linear equations based on Bi-Laplacian operators to calculate the upper and lower envelopes of the given image, which are treated as functions defined over planar domain.

Given an image $\mathbf{I}(x, y)$ with the size of $m \times n$, $\mathbf{I}(x, y)$ can be decomposed by BEMD and presented as

$$\mathbf{I}(x, y) = \sum_{k=1}^{K} \mathrm{IMF}_k(x, y) + \mathbf{r}_K(x, y), \tag{4}$$

where K is the total number of the IMFs, IMF_k is the kth IMF, $\mathbf{r}_K$ is the final residue of the image. The fine-scale details are expressed in the leading IMFs, while the smoothed features are in the remaining IMFs.

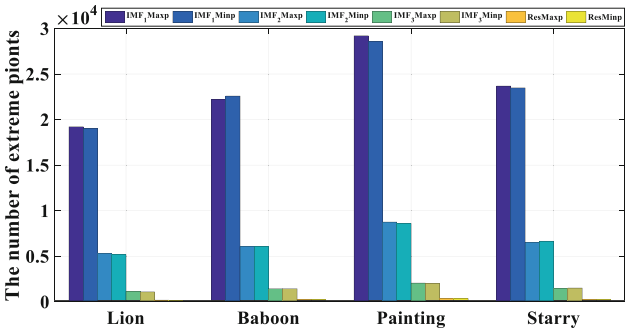

Fig. 2 The number of extreme points of each IMF and the residue for different images

3.3 Watermark embedding

Embedding Region Selection. Embedding region plays an important role in watermark algorithm and directly determines the invisibility and the robustness of the algorithm. It is necessary to carefully select the properly embedding regions. According to the studies of the special property of HVS in [11], signal embedding into the planar region area would be more visible than embedded into the highly textured areas. That is because hiding information in the high frequency of an image yields less humanly detectable perturbations than hiding in the flat regions [4]. Motivated by these observations and the masking property of texture in HVS, the texture regions of the image will be selected as the embedding regions.

The texture components can be extracted from image via the sifting process of BEMD, and are well characterized in the first IMF, denoted by IMF_1. In the sifting process, extreme points play a vital role for determining the upper and lower envelopes, which inspire us to explore using the extreme points in IMF_1 as the watermark embedding positions. Figure 2 shows the number of extreme points in each IMF of different images after BEMD decomposition. From Fig. 2, we can observe that for different images the numbers of maximum points almost equal to the number of minimum points in each IMF and the residue, while the number of the extreme points decrease quickly from the first IMF to the residue. In order to find certain number of embedding positions, the extreme points simultaneously appearing at the first two IMFs are finally selected as the embedding positions, which usually locate on the texture regions and characterize the texture details.

Circular Watermark Embedding. In the watermark embedding process, watermark image $\mathbf{W}(x, y)$ is first transferred into one-dimensional signal $\mathbf{W}_h$ by Arnold transform and Hilbert curve. At the same time, the host image $\mathbf{I}(x, y)$ is decomposed into several IMFs and a residue by BEMD. Then, the extreme points in the first IMF are selected as the embedding positions. Following these ideas, our watermark embedding algorithm is developed by the following schemes.

For the one-dimensional binary signal $\mathbf{W}_h(i), i = 1, \ldots, N \times N$, if $\mathbf{W}_h(1) = 1$, it will be embedded into the maximum position of IMF_1. That is the first maximum point in the extreme point set, which will be selected as the embedding position. If signal $\mathbf{W}_h(1) = 0$, the first minimum point is used as the embedding position. For both of the two cases, the value of IMF_1 in corresponding position is modified by

$$\mathrm{IMF}_1'(x, y) = (1 + \alpha) \times \mathrm{IMF}_1(x, y), \tag{5}$$

where α is a weighting factor balancing a trade-off between the robustness and the imperceptibility of the embedded watermark. Furthermore, α increases the absolute values of extreme points and makes extreme point more stable after watermark embedding. We shall repeat this procedure until all watermark signals are embedded into the extreme positions.

Usually, the size of the host image and total number of extreme points extracted from the IMF_1 are much larger than the size of the watermark image, which enables us to repeatedly embed the watermark signal into the IMF_1 more than two times. Taking the Baboon and the Unity as an example, the number of minimum extreme points is 1666, while the number of zeros in Unity is 628. Therefore, the watermark signal can be embedding in these extreme points two times. Repeatedly embedding will lead to more extracted watermark images. Combining the multiple extracted watermark images into one final watermark image enables the algorithm to be more robust to various attacks.

If the size of the watermark image is 64×64, it may not be completely embedded into IMF_1 once for the limited number of extreme points. The incomplete embedding certainly leads to incomplete extraction. In order to overcome the embedding capacity problem, the repeatedly embedding scheme can be further enhanced by repeating the whole embedding procedure several times. Figure 3a shows a host image with the size of 12×12 and four minimum points and nine maximum points are detected in the first IMF. Fig. 3b is a binary letter 'J' with size of 4×4, and there are eight zero pixels and eight one pixels. All ones can be embedded into the maximum positions, however, just four zeros can be embedded due to the limited number of minimum positions. To embed the remaining zeros, the second time embedding is executed. In the second time embedding, the remaining four zeros are completely embedded in the host image, and all ones are repeatedly embedded simultaneously. The result after twice embedding is shown in Fig. 3d. This scheme is called circular embedding in this paper, which not only solves the embedding capacity problem, but also further enhances our algorithm against more severe attacks. The advantages of the scheme will be further illustrated in watermark extraction.

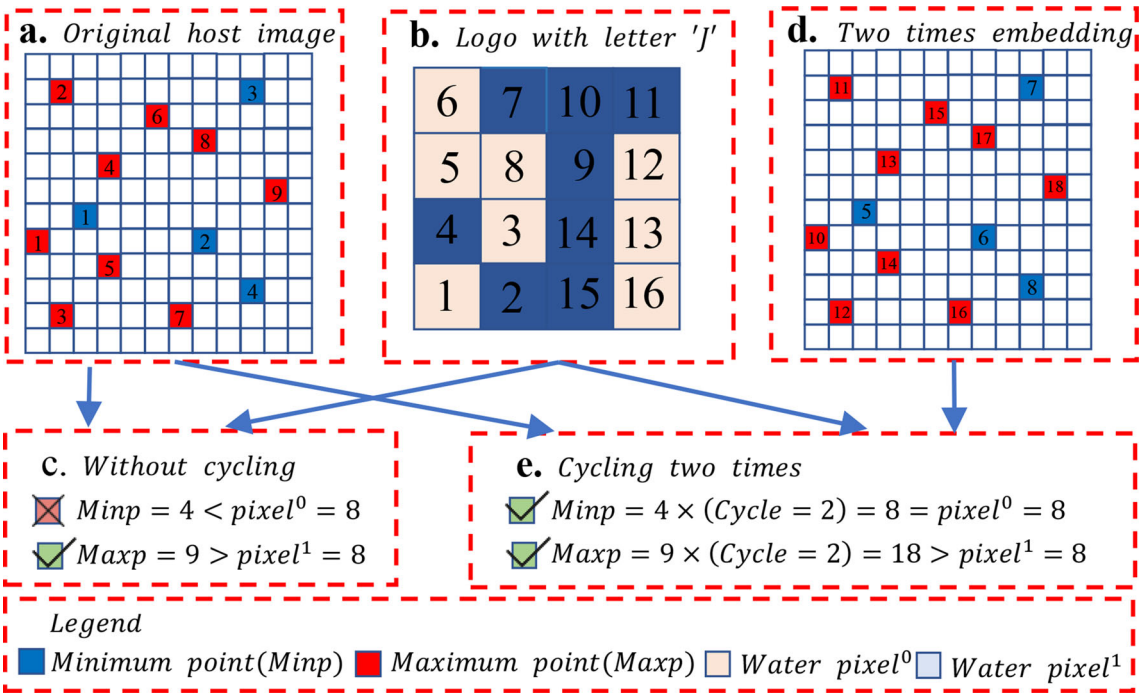

Fig. 3 Circular embedding. **a** Host image. Blue pixels represent the minimum positions of the host image and red pixels represent the maximum positions, respectively. **b** Binary image with a letter $'J'$. **c** Without circular embedding. **d** Host image after twice embedding. **e** The analysis of two times of cycle embedding

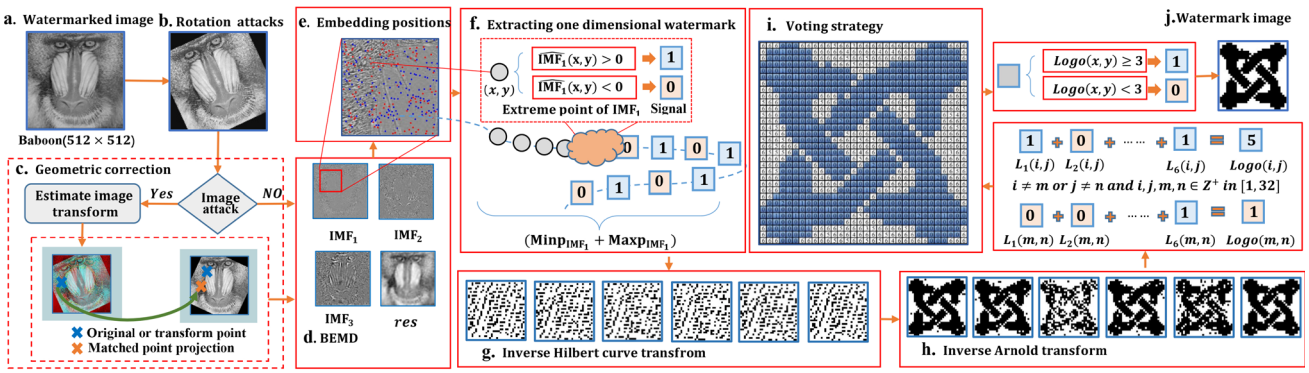

Fig. 4 Pipeline of watermark extraction. **a** Watermarked image. **b** Rotation attacks. **c** Image correction. **d** Obtained IMFs and a residue by BEMD. **e** Embedding positions. **f** One-dimensional watermark extraction. **g** Inverse Hilbert curve. **h** Inverse Arnold transform. **i** Voting strategy. **j** Final extracted watermark image

After circular embedding of the one-dimension signal $\mathbf{W}_h$ into the IMF_1 of the host image, the watermarked image $\mathbf{I}_w(x, y)$ is obtained by combining all IMFs and the residue together with $\mathrm{IMF}_1^{'}$

$$\mathbf{I}_w(x, y) = \mathrm{IMF}_1^{'}(x, y) + \sum_{k=2}^{K} \mathrm{IMF}_k(x, y) + \mathbf{r}_K(x, y). \quad (6)$$

In the watermark embedding process, the iteration number of Arnold transform, the positions of extreme points and circular embedding times are saved for watermark extraction. Figure 1j shows the watermarked baboon with the watermark image unity.

3.4 Watermark extraction

Consider the watermarked image $\mathbf{I}_w(x, y)$ (Fig. 4a), which might be modified by geometric attacks, such as the rotation attack (Fig. 4b). Due to the fact that the watermark has been embedded into the extreme points of IMF_1 decomposed from

the host image $\mathbf{I}(x, y)$, the watermarked image $\mathbf{I}_w(x, y)$ is firstly decomposed by BEMD into IMFs to obtain the first IMF of the watermarked image, denoted as $\widehat{\text{IMF}}_1$. Then, one-dimensional signal can be naturally extracted by checking the attributes of the saved embedding positions corresponding to $\widehat{\text{IMF}}_1$. To reconstruct the watermark image, the reverse Hilbert curve and Arnold transform are performed on the one-dimensional signal. Since the circular embedding scheme is adopted, multiple watermark images are extracted and will be further combined to the final watermark image by the voting strategy. The flowchart of the watermark extraction is illustrated in Fig. 4 and the procedures are presented in Algorithm 1.

Algorithm 1 Watermark Extraction.

Input: Watermarked image $\mathbf{I}_w(x, y)$
Output: Extracted watermark $\mathbf{W}_e(x, y)$
1: Decompose the watermarked image $\mathbf{I}_w(x, y)$ by BEMD and obtain the $\widehat{IMF}_1$;
2: Extract the one-dimensional signal by checking the attributes of the saved embedding positions from $\widehat{IMF}_1$;
3: Perform the inverse Hilbert curve and inverse Arnold transform on the one-dimensional signal and obtain multiple watermark images;
4: Combine the multiple watermark images to the final watermark image $\mathbf{W}_e(x, y)$ by the voting strategy.

One-Dimensional Signal Extraction. It is natural to check the attributes of the embedding positions of $\widehat{\text{IMF}}_1$, as the watermark image has been embedded in these extreme positions. A large number of experiments show that the extreme points still retain the extreme attributes in the first IMF of the watermarked image without any attacks, and the watermark image can be accurately recovered. Nonetheless, the extreme points could not be well preserved under large-scale attacks. The reason is that the attacks modify the value of the watermarked image, which directly destroys the extreme relationship in the decomposed IMFs. Therefore, the watermark image could not be extracted accurately after attacks by directly checking the extremum attributes of the embedding positions.

Fortunately, we have observed that signs of the embedding extreme points are extraordinarily stable and can be well preserved under large-scale attacks from a considerable number of experiments. Taking the maximum point as example, the sign of the maximum point is positive before embedding watermark, and the value of the maximum point has been further enhanced in watermark embedding according to Eq. 5, which results in the well preservation of the positive sign of the maximum point in the first IMF of the watermarked image, in spite of the possibility of serious attacks. This situation can also be observed from the minimum points. Therefore, to achieve stable watermark extraction results, the one-dimensional signal is extracted by performing the following rule: if the sign of $\widehat{\text{IMF}}_1$ in embedding position is positive, the binary 1 is extracted; if the sign of $\widehat{\text{IMF}}_1$ in embedding position is negative, the binary 0 is extracted (see Fig. 4f). After inverse Hilbert curve and inverse Arnold transformation, multiple watermark images are obtained (see Fig. 4h).

Combining Multiple Watermark Images. Watermark image has been repeatedly and circularly embedded in the host image, thus multiple watermark images are extracted. As described earlier, the watermark of Unity is embedded two times in the host image of Baboon. Performing three times of circular embedding, six watermark images are extracted (Fig. 4h). To obtain the final combined watermark image, the voting strategy is adopted. Specifically, the multiple extracted watermark images are added together to obtain the combined watermark image. Then, the pixel value of watermark image is set to be 1 if the value of the combining watermark image in the corresponding position is larger than half of the number of the extracted watermark images; otherwise the pixel value of watermark image is set to be 0. The voting strategy guarantees the algorithm to be more resistant to high-intensity attacks.

Image Correction. Apart from attacks by the traditional image processing filters, the watermarked image might be attacked by geometric transformation, such as rotation, translation, and scaling. Developing a new watermarking algorithm resilient and robust to geometric distortion is still a challenging task nowadays. One feasible solution is to perform geometric distortion correction before watermark extraction, which will provide satisfactory results against geometric attacks.

For the watermarked image $I^{'}(x, y)$, $I_g^{'}(x, y)$ is possibly attacked by the geometry transformations, the Speeded-Up Robust Features (SURF) [6] are computed from them respectively, then the corresponding matched pairs of the feature points are calculated using the M-estimator Sample Consensus algorithm [31]. After that the geometric transform matrix is estimated from the match feature pairs and is used to correct the watermarked image corrupted by geometric attacks.

Figure 5 shows the advantage of image correction in watermark extraction. Due to the large-scale rotation, the embedding positions are shifted in a large range, causing important information lost in the extracted watermark image, which results in unrecognized result (see Fig. 5c). Fig. 5d shows the matched feature points between the watermarked image and the rotated image. Fig. 5f shows the detected watermark image after image correction. From the result, we can observe that the watermark image can be completely extracted after the image correction and the NC value is 1.

Table 1 documents more extracted results against various geometry attacks, such as translation, rotation, and scaling. From the table, we can observe that the NC values of the

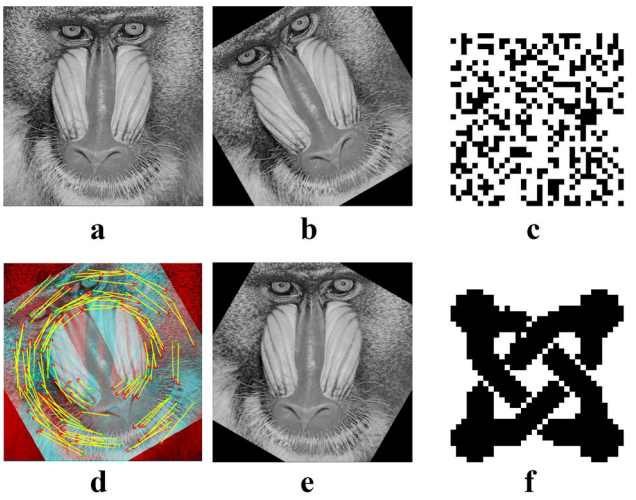

Fig. 5 **a**, **b** Watermarked image and with 30 degree rotation; **c** Result extracted from (**a**); **d** Matching feature points; **e** Corrected image; **f** result extracted from (**e**)

Table 1 Extraction results with or without image correction under geometry attacks

Types	Intensity	No correction	Correction
Rotating	5	0.5095	1.0000
	30	0.5113	1.0000
Translating	Left 100 pixel	0.5126	1.0000
	Up 100 pixel	0.5088	1.0000
Scaling	0.7	0.4802	1.0000
	1.2	0.4907	1.0000

extracted watermark images without image correction are less than 0.52 for three types of geometrical attacks, which means that watermark images cannot be extracted exactly. In contrast, we are pleased to observe that NC values of extracted watermark images after image correction are all ones. Incorporating the geometric distortion correction into the BEMD-based watermark extraction scheme, our method can achieve satisfactory performance and high robustness against various geometric attacks.

4 Experimental results and evaluations

In this section, we first provide the performance measurement and evaluate the main parameters employed in the algorithm. Then, different types of attacks including image processing attacks, various noise attacks, and geometry attacks are considered on the watermarked image to confirm the robustness of the proposed watermarking scheme. At the same time, a large number of experimental results are shown and compared with the state-of-the-art algorithms to exhibit the effectiveness and the advantages of the proposed algorithm.

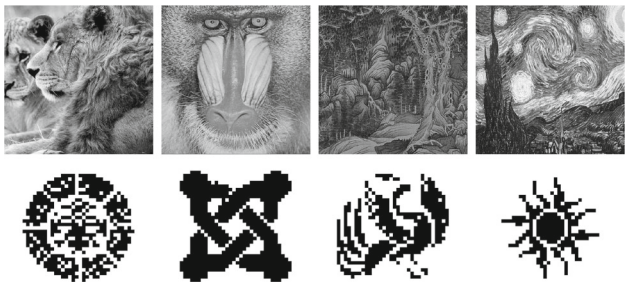

Fig. 6 Host images: from top left to right are Lion, Baboon, Painting and Starry. Watermark images: from bottom left to right are Coin, Unity, Phoenix and Sun

In the experiments, four gray level images with a size of 512×512 are used as original host images and four binary images with a size of 32×32 are used as watermark images (see Fig. 6).

4.1 Performance measurement and parameters

Performance Metrics. In order to demonstrate the imperceptibility of the watermarked image after watermark embedding, the Peak Signal-to-Noise Ratio (PSNR) is employed for evaluating the quality of the watermarked image, which is formulated as

$$\mathrm{PSNR} = 10 \log_{10} \frac{255^2}{\mathrm{MSE}}, \tag{7}$$

and the Mean Square Error (MSE) between the original host image and watermarked image is defined as

$$\mathrm{MSE} = \frac{1}{mn} \sum_{x=1}^{m} \sum_{y=1}^{n} (I(x, y) - I_w(x, y))^2. \tag{8}$$

Imperceptibility indicates an alteration of perceptual watermarked quality of the host image after watermark embedding. In most watermarking research, PSNR value of 40 dB is usually used as the maximum change limit of the embedded image. Table 2 summarizes the PSNR values for various watermarked images without any attack for our newly-proposed watermarking scheme. From this table, we can observe that the PSNR value of watermarked images can reach 54.587 dB after one time embedding. Furthermore, under a lager embedding weighting factor $\alpha = 0.2$, the lowest PSNR value for more cases after four times of circular embedding still remains larger than 38 dB, which indicates that watermarked images have higher imperceptibility.

In order to quantitatively measure the quality of extracted watermark images and confirm the advantages of the circular embedding scheme, the Normalized Cross-correlation (NC) value between the original watermark image and extracted

Table 2 PSNR values between the original host image and the watermarked images without any attack

Host and water	The value of cycle			
	1	2	3	4
Lion+Coin	51.232	44.450	41.315	38.048
Lion+Phoenix	51.273	46.224	42.447	39.004
Lion+Sun	54.587	47.233	42.994	40.240
Baboon+Phoenix	52.717	45.996	41.594	38.331
Baboon+Sun	52.217	46.996	43.275	38.987
Painting+Coin	48.318	43.646	40.605	38.189
Painting+Phoenix	48.403	44.446	41.996	38.990
Painting+Sun	50.596	45.222	43.325	41.272
Starry+Sun	52.390	45.189	41.061	38.291

watermark image is adopted, which is defined as

$$\mathrm{NC} = \frac{\sum_{x=1}^{N}\sum_{y=1}^{N} W(x,y).W_e(x,y)}{\sqrt{\sum_{x=1}^{N}\sum_{y=1}^{N} W(x,y)^2 \sum_{i=1}^{N}\sum_{j=1}^{N} W_e(i,j)^2}}, \quad (9)$$

where N denotes the number of rows and columns for the watermark image, and $W_e(x, y)$ is the extracted watermark image. When the extracted watermark is closer to the original watermark, NC value approximates to 1; otherwise the NC value is between 0 and 1.

Parameter Selection. The watermark image is first scrambled by Arnold transform to improve the security of the watermark image, in which the number of scrambling iteration is recorded and used as the secret key in the inverse Arnold transform. In our experiments, five scrambling iterations are performed.

In watermark embedding process, the weighting factor α plays the role of embedding intensity. Usually, higher value of α can increase the robustness of the algorithm against attacks, while it also reduces the imperceptibility of the watermarked image at the same time. Through a large number of experiments, we find that $\alpha = 0.2$ can produce satisfactory extraction results, and provide the best trade-off between the imperceptibility and the robustness of the algorithm.

Another important parameter is the number of circular times in watermark embedding process. From larger number of experiments, we can observe that the circular embedding scheme equips our algorithm with fantastic capability against more severe attacks within three times of embedding. Therefore, without loss of generality, three times of circular embedding are adopted in the following experiments.

4.2 Robustness evaluations

In Table 3, various attacks are applied to the watermarked images to illustrate the robustness of our algorithm. It can be

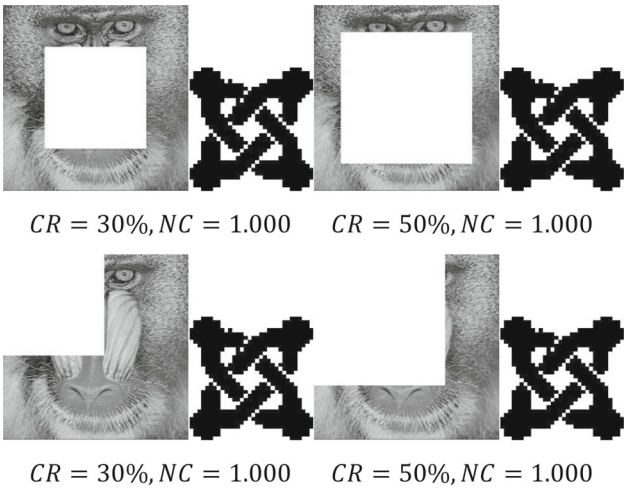

Fig. 7 Results of large-scale cropping, including middle cropping and corner cropping

observed that the NC values of extracted watermark images are all ones under the attacks of Sharpening (SH-R=3), Histogram Equalization (HE-64), Gamma Correction (GC-2 and 0.5), Speckle Noise (SN-0.01), Gaussian Noise (GN-0.01), JPEG Compression (JC-40) and Scaling (SC-4). For the attacks of Pepper and Salt Noise (PN-0.1), our proposed method also has excellent performances and the NC values of them are larger than 0.988. For Median Filtering attack (MF-[3,3]), the NC values of them are around 0.96. These results confirm that the proposed method can obtain satisfactory results and is robust to various attacks. It is also worth noting that most of the PSNR values are greater than 40, which indicates our method also has good imperceptibility.

Figure 7 shows the watermarked images under the large-scale cropping and the corresponding extracted watermark images. It can be seen that the watermark images are completely extracted with 30% cropping from different positions and the NC values of extracted watermark images are all 1. Even after 50% intermediate cropping and corner cropping, the NC values of the extracted watermark images are still ones. The reason of our newly-proposed algorithm can resist large-scale cropping attacks is that, the circular embedding scheme and voting strategy are adopted in the watermark embedding and extraction stages.

4.3 Comparisons with previous algorithms

To further demonstrate the advantages of the newly-proposed method, we extensively compared our method with traditional watermarking algorithms, such as LSB [12], DCT [5] and DWT [16], BEMD-based watermarking algorithms [1, 27], and the hybrid watermarking algorithms [15,23,26,28].

Comparison with Traditional Watermarking Algorithms. Figure 8 illustrates the comparison results between our

Table 3 The NC results the extracted watermark images by applying different attacks

Attacks	Lion				Baboon				Painting			
	Coin	Unity	Phoenix	Sun	Coin	Unity	Phoenix	Sun	Coin	Unity	Phoenix	Sun
GF-[3,3]	1.000	1.000	1.000	1.000	1.000	1.000	1.000	0.999	1.000	1.000	1.000	0.999
MF-[3,3]	0.939	0.914	0.937	0.936	0.984	0.987	0.967	0.965	0.984	0.987	0.967	0.965
WF-[3,3]	1.000	1.000	1.000	1.000	0.964	0.989	0.966	0.943	0.964	0.989	0.966	0.943
AF-[3,3]	1.000	0.995	0.993	0.997	0.984	0.987	0.980	0.963	0.984	0.987	0.980	0.963
SH-R=3	1.000	1.000	1.000	1.000	1.000	1.000	1.000	1.000	1.000	1.000	1.000	1.000
HE-64	1.000	1.000	1.000	1.000	1.000	1.000	1.000	1.000	1.000	1.000	1.000	1.000
GC-2	1.000	1.000	1.000	1.000	1.000	1.000	1.000	1.000	1.000	1.000	1.000	1.000
GC-0.5	1.000	1.000	1.000	1.000	1.000	1.000	1.000	1.000	1.000	1.000	1.000	1.000
PN-0.1	0.998	0.993	0.988	0.999	0.998	1.000	0.998	0.999	0.999	1.000	1.000	1.000
SN-0.01	1.000	1.000	1.000	1.000	1.000	1.000	1.000	1.000	1.000	1.000	1.000	1.000
GN-0.01	1.000	1.000	0.998	0.999	1.000	1.000	1.000	1.000	1.000	1.000	1.000	1.000
JC-40	1.000	1.000	1.000	1.000	1.000	1.000	1.000	1.000	1.000	1.000	1.000	1.000
SC-4	1.000	1.000	1.000	1.000	1.000	1.000	1.000	1.000	1.000	1.000	1.000	1.000
PSNR	41.315	39.784	42.447	42.994	40.317	41.349	41.594	43.275	40.605	35.827	41.996	43.325

PSNR of the watermarked images are listed at the bottom

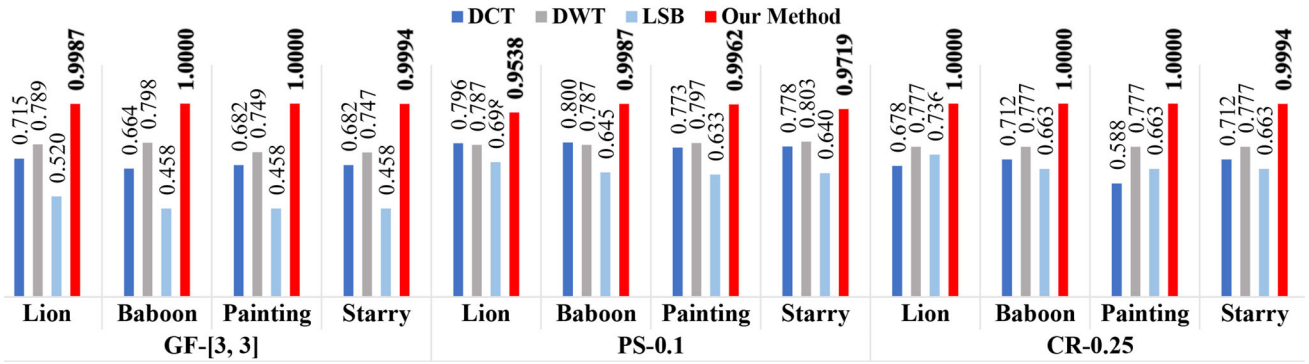

Fig. 8 The NC results of three conventional watermarking methods, DCT [5], DWT [16], and LSB [12], for three types of attacks. GF-[3,3] stands for Gaussian Low-pass filtering [3,3], PS-0.1 represents Pepper and Salt under the intensity of 0.1. CR-0.25 represents cropping attack with 25%

method with LSB, DCT, and DWT under three kinds of attacks, including Gaussian Low-pass Filtering [3, 3], Pepper and Salt (0.1) and cropping the upper left corner (25%). From the results, we can see that our newly-proposed algorithm has better performance than DWT, DCT, and LSB against Pepper and Salt noises, cropping and Gaussian low-pass filtering attacks. The NC values of the extracted watermark images for DWT, DCT, and LSB are all below 0.9, and some of the extracted watermark images can not be well recognized. The NC value for DCT is just 0.5985 under 25% cropping attack. In contrast, the NC values of the extracted watermark images by our algorithm are much higher than the other three algorithms under different attacks. For example, the NC values are all ones for Gaussian noise attack and cropping attack. For Pepper and Salt noise attack, our method also obtains better extracted results, and the NC values of them are larger than 0.997 and one of the value reaches 0.999.

Comparison with BEMD-based Watermarking Algorithms. To further verify the robustness of our newly-proposed algorithm, two BEMD-based watermarking algorithms [1,27] are compared and documented in Table 4. Compared with the two methods [1,27], our new algorithm obtains better performance and has much higher NC values under various attacks. For Gaussian filter attacks, large-scale rotation attacks, 20% cropping attacks, the NC values of our method are all ones, while the other methods obtain lower NC values in comparison with our method.

From Table 4, we can see that the method [27] is not robust to JPEG compression attacks, image filters, and geometry attacks. For a small angle rotation, the NC value of the extracted watermark image by the method [27] is only 0.681. We also notice that most of the NC values of the method [1] are larger than 0.99. However, the method [1] is a non-blind watermark algorithm and the original host image is used in

Table 4 The NC values in comparison with with two BEMD-based watermarking algorithms of the same attack intensity

Attack types	[27]	[1]	Our method
JC-10	0.8360	0.9940	**0.9987**
JC-20	0.8456	0.9950	**0.9989**
JC-30	0.8757	0.9950	**0.9998**
JC-40	0.8816	0.9950	**1.0000**
JC-50	0.8904	0.9950	**1.0000**
PN-0.1	NaN	0.9930	**0.9962**
GF-[2,2]	NaN	0.9950	**1.0000**
GF-[3,3]	0.9590	0.9950	**1.0000**
MF-[2,2]	NaN	**0.9950**	0.9805
MF-[3,3]	0.8760	**0.9940**	0.9276
WF-[2,2]	NaN	0.9950	**1.0000**
WF-[3,3]	0.8619	0.9940	**0.9998**
RO-[-50]	NaN	0.9410	**1.0000**
RO-[-2]	0.7162	0.9930	**1.0000**
RO-[-1]	0.7034	NaN	**1.0000**
RO[1]	0.6942	NaN	**1.0000**
RO-[2]	0.6810	0.9910	**1.0000**
RO-[70]	NaN	0.9820	**1.0000**
CR-10	NaN	0.9900	**1.0000**
CR-20	NaN	0.9900	**1.0000**

Data without the corresponding values are denoted by NaN. The largest value in each line is marked in bold

the watermark extraction process. The above comparisons clearly indicate that the proposed scheme performs better than existing BEMD-based watermarking methods in resistance to most image processing attacks and noise attacks, and especially geometry attacks.

Comparison with Hybrid Watermarking Algorithms. Four hybrid watermarking algorithms, including DCT and Dynamic Stochastic Resonance (DCT-DSR) [28], DWT and Significant Amplitude Difference (DWT-SAD) [23], DFT and DCT (DFT-DCT) [15], Fast Discrete Curvelet Transform and DCT (FDCuT-DCT) [26], are compared comprehensively in order to showcase the performance of our newly-proposed watermarking algorithm. Table 5 shows the NC values of the extracted watermark images from the compared algorithms and our algorithm, respectively. In order to maintain the fairness as much as possible, the same attack intensities are applied to our watermarked images, and the compared NC values are completely referred to the corresponding papers. From the table we can see that, our algorithm has salient advantages under 19 kinds of attacks. Most NC values of extracted watermark images by our algorithm are all ones.

What attracts our attention the most is that, the method [28] is not very good under most kinds of attacks, and all NC values are less than 0.91. The method of [23] has poor performance under JPEG compression attack and the high intensity Pepper and Salt noise. It can not provide copyright protection when the watermarked image has more than 20% cropping. The algorithm [15] obtains higher NC values under cropping attacks, however, this method is not robust to other attacks, especially for JPEG compression and Gaussian noises attacks. Similarly, the method of [26] is also not robust to JPEG compression and Gaussian noises attacks. Moreover, when the watermarked image is attacked by median filtering and average filtering, the NC values of them are lower than 0.46, and the extracted watermark images are hardly recognized. In contrast to these algorithms, the newly-proposed algorithm has strong ability against JPEG compression, Gaussian noises attacks, image filtering attacks, cropping, and geometric attacks.

4.4 Limitation and future work

Although our algorithm has afforded very satisfactory results, it still has a limitation when the host image is containing less texture regions. If the host image contains large plain-region area, there will be less texture area to be embedded during watermark embedding, which will give rise to lower imperceptibility and less robustness to various attacks. To ameliorate, following the idea of hiding images within images [4], we will explore new non-embedding schemes to overcome this limitation, which will not modify the host image, and do not rely on the texture complexity of the host image as much as possible.

5 Conclusion

In this paper, we have proposed a robust, blind image watermarking algorithm by taking the advantage of Hilbert curve, BEMD, and circular embedding scheme. For the watermark image, it is scrambled by Arnold transform to increase its security and then reduced to a one-dimensional signal by Hilbert curve. For host image, it is decomposed using BEMD to obtain the first IMF, which characterizes the texture regions of the host image. Then, the one-dimensional watermark signal is repeatedly and cyclically embedded into the extreme points of the first IMF to achieve better performance. The circular embedding scheme not only increases the embedding capacity, but also enhances the robustness of the algorithm against various attacks. Finally, the watermark can be effectively extracted without using the original host image. In addition, to combat the potential geometric attacks, image correction will be optionally applied to the watermarked image before watermark extraction. A large number of experimental results and comparisons with previous algorithms have confirmed that our method can obtain higher imper-

Table 5 The NC results in comparison with experiments of four hybrid watermarking algorithms

Attack types	DCT- DSR [28]	DWT- SAD [23]	DFT- DCT [15]	FDCuT- DCT [26]	Our method
JC-10	0.8639	0.6300	0.6743	NaN	**0.9833**
JC-20	0.8758	0.8500	0.7890	NaN	**0.9987**
JC-30	0.8750	0.9200	0.9947	NaN	**1.0000**
JC-40	0.8758	0.9700	0.9344	0.9597	**1.0000**
JC-50	0.8754	0.9900	0.9626	0.9639	**1.0000**
PN-0.01	0.8742	0.9863	0.9609	0.9843	**1.0000**
PN-0.1	0.8978	0.8634	NaN	0.8314	**0.9917**
PN-0.3	0.8782	NaN	NaN	NaN	**0.9459**
GN-0.005	0.8897	NaN	0.9947	0.9922	**1.0000**
GN-0.01	0.9012	NaN	NaN	0.9500	**1.0000**
GN-0.02	0.8764	NaN	NaN	0.8832	**1.0000**
GN-0.1	0.9538	NaN	NaN	0.6827	**0.9968**
GN-0.15	0.9022	NaN	NaN	NaN	**0.9949**
GF-[3,3]	0.8873	0.9900	0.9954	0.9916	**1.0000**
MF-[3,3]	0.9091	0.9300	NaN	0.4576	**0.9853**
AF-[3,3]	0.8737	NaN	NaN	0.2258	**0.9994**
CR-10%	0.8839	NaN	**1.0000**	0.9795	**1.0000**
CR-20%	0.8825	0.8800	NaN	NaN	**1.0000**
CR-25%	0.8837	NaN	**1.0000**	NaN	**1.0000**

Data without the corresponding values are denoted by NaN. The largest value in each line is marked in bold

ceptibility and robustness under different types of attacks, including image processing attacks, various noises attacks, image enhancement attacks, and especially, the challenging geometric attacks.

Funding Information This research is supported in part by National Science Foundation of USA (IIS-1715985 and IIS-1812606), National Natural Science Foundation of China (No. 61672149, 61602341, 61672077, 61532002, 61602344, 61802279, 61872347); Natural Science Foundation of Tianjin (18JCQNJC00100). The Science & Technology Development Fund of Tianjin Education Commission for Higher Education (Grant No. 2018KJ222).

Compliance with ethical standards

Conflict of interest The authors declare no conflict of interest.

References

1. Abbas, N.H., Ahmad, S.M.S., Parveen, S., Wan, W.A., Ramli, A.R.B.: Design of high performance copyright protection watermarking based on lifting wavelet transform and bi empirical mode decomposition. Multimed. Tools Appl. **77**(19), 24593–24614 (2018)
2. Abdelouahed, S., Mohamed, K., Hamid, T., Aabdelah, A.: Image watermarking using the empirical mode decomposition. In: 5th International Conference Science Electronics, Tech. Info. Telecom., pp. 22–26 (2009)
3. Ali, M., Ahn, C.W., Pant, M., Siarry, P.: An image watermarking scheme in wavelet domain with optimized compensation of singular value decomposition via artificial bee colony. Inform. Sci. **301**, 44–60 (2015)
4. Baluja, S.: Hiding images within images. IEEE Trans. Pattern. Anal. Mach. Intell. **42**(7), 1685–1687 (2019)
5. Barni, M., Bartolini, F., Cappellini, V., Piva, A.: A dct-domain system for robust image watermarking. Signal Process. **66**(3), 357–372 (1998)
6. Bay, H., Ess, A., Tuytelaars, T., Gool, L.V.: Speeded-up robust features (surf). Comput. Vis. Image Underst. **110**(3), 346–359 (2008)
7. Bi, N., Sun, Q., Huang, D., Yang, Z., Huang, J.: Robust image watermarking based on multiband wavelets and empirical mode decomposition. IEEE Trans. Image Process. **16**(8), 1956–1966 (2007)
8. Celik, M.U., Sharma, G., Tekalp, A.M., Saber, E.: Lossless generalized-lsb data embedding. IEEE Trans. Image Process. **14**(2), 253–266 (2005)
9. Chen, B., Coatrieux, G., Chen, G., Coatrieux, J.L., Shu, H.: Full 4-d quaternion discrete fourier transform based watermarking for color images. Digit. Signal Process. **28**, 106–119 (2014)
10. Chu, W.C.: Dct-based image watermarking using subsampling. IEEE Trans. Multimed. **5**(1), 34–38 (2003)
11. Cox, I.J., Miller, M.L.: A review of watermarking and the importance of perceptual modeling. In: Proceedings of Electronic Imaging, pp. 92–99 (1997)
12. Deepshikha, C., Preeti, G., Gaur, S.B., Anil, G.: Lsb based digital image watermarking for gray scale image. IOSR J. Comput. Eng. **6**(1), 36–41 (2012)
13. Di, C., Yang, X., Wang, X.: A four-stage hybrid model for hydrological time series forecasting. PLoS ONE **9**(8), e104–e663 (2014)
14. Fan, M.Q., Wang, H.X., Li, S.K.: Restudy on svd-based watermarking scheme. Appl. Math. Comput. **203**(2), 926–930 (2008)

15. Hamidi, M., Haziti, M.E., Cherifi, H., Hassouni, M.E.: Hybrid blind robust image watermarking technique based on dft-dct and arnold transform. Multimed. Tools Appl. **77**(20), 27181–27214 (2018)
16. Hernandez-Guzman, V., Cruz-Ramos, C., Nakano-Miyatake, M., Perez-Meana, H.: Watermarking algorithm based on the dwt. IEEE Lat. Am. Trans. **4**(4), 257–267 (2006)
17. Hilbert, D.: Über die stetige abbildung einer linie auf ein flächenstück. Math. Ann. **38**(3), 459–460 (1891)
18. Hu, J., Wang, X., Qin, H.: Improved, feature-centric emd for 3d surface modeling and processing. Graph. Models **76**(5), 340–354 (2014)
19. Hu, J., Wang, X., Qin, H.: Novel and efficient computation of hilbert huang transform on surfaces. Comput. Aided Geom. Des. **43**, 95–108 (2016)
20. Huang, N.E., Shen, Z., Long, S.R., Wu, M.C., Shih, H.H., Zheng, Q., Yen, N.C., Tung, C.C., Liu, H.H.: The empirical mode decomposition and the hilbert spectrum for nonlinear and non-stationary time series analysis. Proc. Math. Phys. Eng. Sci. **454**(1971), 903–995 (1998)
21. Hussein, M., Bairam, M.: A survey study on singular value decomposition and genetic algorithm based on digital watermarking techniques. In: Proceedings of Firs International Conference Computer International Info., pp. 7–16 (2017)
22. Lai, C.C.: A digital watermarking scheme based on singular value decomposition and tiny genetic algorithm. Digit. Signal Process. **21**(4), 522–527 (2011)
23. Li, C., Zhang, Z., Wang, Y., Ma, B., Huang, D.: Dither modulation of significant amplitude difference for wavelet based robust watermarking. Neurocomputing **166**, 404–415 (2015)
24. Roy, S., Pal, A.K.: A robust blind hybrid image watermarking scheme in rdwt-dct domain using arnold scrambling. Multimed. Tools Appl. **76**(3), 3577–3616 (2017)
25. Sagan, H.: A three-dimensional hilbert curve. Int. J. Math. Educ. Sci. Tech. **24**(4), 541–545 (1993)
26. Seyyed, H.S., Amir, H.T., Amir, H.M.: Waca: a new blind robust watermarking method based on arnold cat map and amplified pseudo-noise strings with weak correlation. Multimed. Tools Appl. **78**(14), 19163–19179 (2019)
27. Sharma, J.B., Sharma, K.K., Sahula, V.: Digital image dual watermarking using self-fractional Fourier functions, bivariate empirical mode decomposition and error correcting code. J. Opt. **42**(3), 214–227 (2013)
28. Singh, S.P., Bhatnagar, G.: A new robust watermarking system in integer dct domain. J. Vis. Commun. Image R **53**, 86–101 (2018)
29. Subr, K., Soler, C., Durand, F.: Edge-preserving multiscale image decomposition based on local extrema. ACM Trans. Graph. **28**(5), 1471–1479 (2009)
30. Tao, P., Eskicioglu, A.M.: A method for image recovery in the dft domain. In: 3rd IEEE Cons. Comm. Network. Conf., vol. 2, pp. 1134–1138 (2006)
31. Torr, P., Zisserman, A.: Mlesac: a new robust estimator with application to estimating image geometry. Comput. Vis. Image Underst. **78**(1), 138–156 (2000)
32. Tsui, T.K., Zhang, X.P., Androutsos, D.: Color image watermarking using multidimensional Fourier transforms. IEEE Trans. Inf. Forensics Secur. **3**(1), 16–28 (2008)
33. Wang, H., Su, Z., Cao, J., Wang, Y., Zhang, H.: Empirical mode decomposition on surfaces. Graph. Models **74**(4), 173–183 (2012)
34. Wang, X., Hu, J., Guo, L., Zhang, D., Qin, H., Hao, A.: Feature-preserving, mesh-free empirical mode decomposition for point clouds and its applications. Comput. Aided Geom. Des. **59**, 1–16 (2018)
35. Wang, X., Hu, J., Zhang, D., Guo, L., Qin, H., Hao, A.: Multi-scale geometry detail recovery on surfaces via empirical mode decomposition. Comput. Graph. **70**, 118–127 (2018)
36. Wang, X., Hu, J., Zhang, D., Qin, H.: Efficient emd and hilbert spectra computation for 3d geometry processing and analysis via space-filling curve. Vis. Comput. **31**(6), 1135–1145 (2015)
37. Wang, Y., Doherty, J.F., Van Dyck, R.E.: A wavelet-based watermarking algorithm for ownership verification of digital images. IEEE Trans. Image Process. **11**(2), 77–88 (2002)
38. Xie, X.: Illumination preprocessing for face images based on empirical mode decomposition. Signal Process. **103**, 250–257 (2014)
39. Zhang, D., Wang, X., Hu, J., Qin, H.: Interactive modeling of complex geometric details based on empirical mode decomposition for multi-scale 3d shapes. Comput. Aided Des. **87**, 1–10 (2017)

Xiaochao Wang is an associate professor in School of Mathematical Sciences at Tiangong University. He received his PHD degree in Computational Mathematics from Dalian University of Technology in 2014. His research interests include computational geometry, computer graphics, and image processing.

Kun Hu received the B.S. degree from Tiangong University. He is currently pursuing the M.S. degree with the Technology and Engineering Center for Space Utilization, Chinese Academy of Sciences, China. His research interests include image processing and spacecraft orbit design and attitude control.

Jianping Hu is a professor in College of Science at School of Sciences at Northeast Electric Power University. He obtained his BS and MS in Mathematics at Jilin University. He received his PhD in Computational Mathematics from Dalian University of Technology in 2009. His research interests include computational geometry, computer graphics, and image processing and analysis.

Ling Du is a lecture in School of Computer Science and Technology at Tiangong University. Her received the B.E. and M.E. degrees in computer science from Liaoning University, Shenyang, China, and the Ph.D. degree with the School of Computer Science and Technology, Tianjin University in 2016, Tianjin, China. Her current research interests include multimedia information security digital watermarking, and image processing.

Anthony T.S. Ho is a professor of Department of Computer Science, University of Surrey, UK. He received the BSc(Hons) in Physical Electronics from Northumbria University in 1979, and his MSc in Applied Optics from Imperial College London in 1980 and his PhD in Digital Image Processing from King's College London in 1983. His research interests include multimedia security, digital watermarking, and image processing.

Hong Qin is a full professor of Computer Science in Department of Computer Science at Stony Brook University (SUNY). He received the B.S. and M.S. degrees from Peking University, and the Ph.D. degree from the University of Toronto, all in computer science. His research interests include geometric and solid modeling, graphics, physics-based modeling and simulation, computer-aided geometric design, visualization, and scientific computing.